Efficient two-process frequency conversion through a dark intermediate state

Gil Porat* and Ady Arie

Department of Physical Electronics, Fleischman Faculty of Engineering, Tel Aviv University, Tel Aviv 69978, Israel
**Corresponding author: gilpor@gmail.com*

Received July 9, 2012; accepted August 21, 2012;
posted August 27, 2012 (Doc. ID 172053); published September 24, 2012

Two simultaneous three wave mixing processes are analyzed, where an input frequency is converted to an output frequency via an intermediate stage. By employing simultaneous phase-matching and an adiabatic modulation of the nonlinear coupling strengths, the intermediate frequency is kept dark throughout the interaction while obtaining high conversion efficiency. This feat is accomplished in a manner analogous to population transfer in atomic stimulated Raman adiabatic passage. Applications include conversion between remote frequencies, e.g., mid-IR to visible, and study of electronic crystal properties in the UV absorption band. © 2012 Optical Society of America

OCIS codes: 190.4223, 190.4410.

1. INTRODUCTION

Quadratic nonlinear optical media are commonly used to perform optical frequency conversion via three wave mixing (TWM) processes [1]. In this way, laser frequencies that are not available by direct laser action are generated. Combinations of such processes were utilized extensively in order to reach frequencies either far removed from a laser source or close to it [2,3]. This task is not trivial, since in order for a TWM process to be efficient a phasematching condition has to be fulfilled. For a single TWM process, a well known solution is quasi-phase-matching (QPM) [4,5], e.g., by periodically modulating the sign of the nonlinear coefficient. Schemes also exist for simultaneous phase-matching of multiple processes [6,7], at the expense of conversion efficiency. Furthermore, the medium is required to be transparent at all participating frequencies, including any frequency generated as an intermediate stage before further conversion.

Recently, analogies were shown between the dynamics of simultaneous TWM processes and those induced in three level atoms by electromagnetic fields. In one publication, an analogy is utilized to perform second harmonic generation and sum frequency generation (SFG) simultaneously, such that the third harmonic is generated efficiently [8]. In this case, the dynamics is nonlinear; i.e., the wave-coupling is a dynamic variable, and significant power was generated at the intermediate frequency (second harmonic). In another work the analogy was applied to the case of purely linear dynamics, where two simultaneous sum or difference generation processes (DFG), or a combination of them, were performed under the constant (undepleted) pump approximation [9]. With this method, called adiabatic elimination, only negligible power is ever present at the intermediate frequency throughout the entire conversion process, so transparency at the intermediate frequency is not required. However, this method explicitly requires that each one of the two processes has a large phase-mismatch. Because of inherently large phase-mismatches, high conversion efficiency is difficult to achieve, and requires high pump intensities or very long interaction lengths.

Here, we propose a method to perform two simultaneous TWM processes efficiently and without significant generation of an intermediate frequency. In contrast to adiabatic elimination [9], the two processes are phase-matched throughout the entire interaction length. High efficiency can therefore be maintained even in the presence of significant absorption of the intermediate frequency wave. As a result, one of the nonlinearity enhancement mechanisms that is associated with absorption resonances can be exploited. In this case, the analogous atomic scenario is the so-called stimulated Raman adiabatic passage (STIRAP) [10,11]. We emphasize that here the dynamics are linear, in complete correspondence to STIRAP. It is this linearity that enables the elimination of the intermediate frequency, in contrast to the previous work by Longhi [8], which mimicked a nonlinear version of STIRAP, and consequently significant intermediate power was present (~20% of the input power).

The insensitivity to intermediate frequency absorption makes possible processes in which the intermediate frequency is in the ultraviolet (UV) absorption band of a nonlinear crystal. This method can thus be used to probe the electronic properties of the crystal in this spectral region, a task that was previously made difficult by absorption.

In order to avoid confusion, we stress that the physical processes considered in this work are fundamentally different from those based on energy transfer between ions, such as excited state absorption, energy transfer upconversion, cooperative sensitization, etc. [12]. In these processes, ions are pumped to excited states, exchange energy, and decay radiatively. This kind of interaction is limited to optical frequencies coinciding with ionic or atomic resonances. Here we consider parametric processes involving virtual states, i.e., atoms stay essentially in the same state, experiencing only small perturbations. These processes can involve any frequency in the transparency range of the nonlinear medium, which usually stretches from the near UV to the mid-IR.

This paper is organized as follows. In Section 2, the theoretical model is presented and adiabatic interaction is analyzed. In Section 3, two study cases, which demonstrate the main features of our method, are simulated numerically assuming ideal conditions. Section 4 repeats the calculation of Section 3 under conditions that are attainable with current QPM technology, and discusses its limitations. In Section 5 we discuss further improvements of the QPM-based method and another way of achieving nonlinear optics STIRAP, as well as applications of this technique.

2. THEORETICAL MODEL AND ANALYSIS

A. Theoretical Model and Atomic Analogy

In this model, two simultaneous TWM processes are considered, such that the frequency generated by one process is further combined with another frequency in the other process. For example, a SFG process $\omega_2 = \omega_1 + \omega_{p_1}$ can be accompanied by a DFG process $\omega_3 = \omega_2 - \omega_{p_2} = \omega_1 + \omega_{p_1} - \omega_{p_2}$, where ω_1 is the input frequency, ω_2 is the intermediate frequency, ω_3 is the output frequency, and ω_{p_1} and ω_{p_2} are the first and second pump frequencies, respectively. We use the constant pump approximation: The two pump waves are taken to be much more intense than the other waves and thus they are negligibly affected by the interaction. Furthermore, all beams are assumed to be plane waves. If one uses Gaussian beams, this requirement can be translated to a Rayleigh range z_R that satisfies $z_R \gtrsim L/2$, where L is the nonlinear medium's length. Finally, we also assume that no other mixing process has any significant effect, due to a large phase-mismatch value. Further details on the validity of this assumption is given in the next subsection.

The corresponding coupled wave dynamics equations for this scenario are

$$i\frac{d}{dz}|\psi\rangle = M|\psi\rangle, \tag{1}$$

where $|\psi\rangle = [A_1, A_2, A_3]^T$ is the state vector, in which $\psi_j = A_j(z)$ is the complex envelope of the amplitude of the wave with frequency ω_j, and

$$M = -\begin{bmatrix} 0 & \kappa_{12}e^{-i\Delta k_1 z} & 0 \\ \kappa_{21}e^{i\Delta k_1 z} & 0 & \kappa_{23}e^{-i\Delta k_2 z} \\ 0 & \kappa_{32}e^{i\Delta k_2 z} & 0 \end{bmatrix} \tag{2}$$

is the coupling matrix. Here $\kappa_{12} = [\chi^{(2)}(\omega_1, \omega_{p_1}; \omega_2)\omega_1^2/k_1c^2][\mathrm{Re}\{A_{p_1}\} \mp i\,\mathrm{Im}\{A_{p_1}\}]$ and $\kappa_{23} = [\chi^{(2)}(\omega_2, \omega_{p_2}; \omega_3)\omega_2^2/k_2c^2][\mathrm{Re}\{A_{p_2}\} \mp i\,\mathrm{Im}\{A_{p_2}\}]$, where $\kappa_{ij} = (\omega_i^2 k_j/\omega_j^2 k_i)\kappa_{ji}^*$ are the effective coupling coefficients between the fields. A_{p_1} and A_{p_2} are the complex envelopes of the amplitudes of the pumps fields, $\chi^{(2)}$ is the second-order nonlinear coefficient of the material, and c is the velocity of light. $\Delta k_1 = k_1 \pm k_{p_1} - k_2$ and $\Delta k_2 = k_2 \pm k_{p_2} - k_3$ are the phase mismatches of the two nonlinear processes, where $k_j = n_j(\omega_j)\omega_j/c$ is the wavenumber of the wave with frequency ω_j. The constant pumps approximation $dA_{p_1}/dz = dA_{p_2}/dz = 0$ is included implicitly. These equations can describe four different cases: two SFG processes, two DFG processes, SFG followed by DFG, and DFG followed by SFG (see Fig. 1). The difference between these processes is manifested in the choice of either the top or bottom sign in κ_{ij} and Δk_j. The top sign corresponds to SFG, while the bottom sign corresponds to DFG.

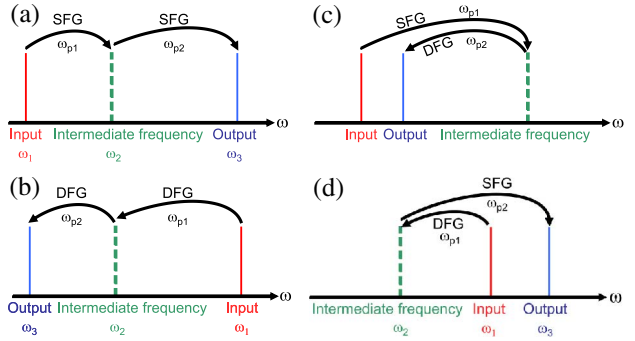

Fig. 1. (Color online) Four cases described by Eq. (1): (a) two SFG processes, (b) two DFG processes, (c) SFG followed by DFG, and (d) DFG followed by SFG.

These equations are isomorphic to the dynamics equations of a three level atom interacting with two EM fields [10,11]: The optical interaction takes place over space (the z axis in our notation), while the atomic interaction takes place over time. The complex amplitude of each field A_j corresponds to the probability amplitude of population in each atomic state, often denoted a_j. Each effective coupling coefficient κ_{ij} is the counterpart of the dipole coupling strength between atomic levels i and j, usually described using the Rabi frequency $\Omega_{ij}(t) = d_{ij} \cdot \varepsilon(t)/\hbar$, where d_{ij} is the dipole moment between levels i and j, $\varepsilon(t)$ is the induced EM field, and $\hbar$ is the reduced Planck's constant. Finally, the phase mismatches, Δk_1 and Δk_2, correspond to the detunings with the two atomic transitions, Δ_1 and Δ_2, respectively. We note one minor difference: Because of symmetry considerations, in the three level atom $\Omega_{ij} = \Omega_{ji}^*$ when the two coupling lasers have the same peak intensity, while in the nonlinear optics case $\kappa_{ij} = (\omega_i^2 k_j/\omega_j^2 k_i)\ \kappa_{ji}^* \neq \kappa_{ji}^*$, as noted above.

As explained and demonstrated in previous works [13], these equations, which assume quasimonochromatic laser beams for the optical case, are applicable to pulses as short as 1 ps, owing to the mismatch between the group velocities of the different interacting wavelengths. Shorter pulses can be stretchered before the interaction and compressed to their transformed limited duration after the interaction [14].

B. Analysis of Interaction Under Adiabatic Variation

A brief description of atomic STIRAP will be given here, while a more rigorous analysis will be performed for the nonlinear optics variant. In atomic STIRAP [10,11], atomic population is transferred from an initial state to a final state, where there is no dipole coupling between these two states. Rather, each of these two states is dipole-coupled to an intermediate state. Interestingly, STIRAP achieves this population transfer without ever having significant population in the intermediate state. This feat is accomplished by adiabatically varying the Rabi frequencies $\Omega_{ij}(t)$ via control over the temporal shape of the induced EM field $\varepsilon(t)$ or using time varying detunings $\Delta_j(t)$. Specifically, a pulse that couples the intermediate and final state is introduced into the atomic system, followed by another pulse that couples the intermediate state with the initial state, such that these two pulses have some temporal overlap. Only when this counterintuitive pulse order is used is STIRAP achieved and the intermediate state remains

unpopulated. This absence of population in the intermediate state renders the population transfer insensitive to radiative losses that may result from the short life time of the intermediate state; hence in this context it is termed a "dark state." In an optimal atomic STIRAP process all of the initial state population has been transferred to the final state, without suffering any loss. Optimization of the atomic STIRAP process by temporally shaping $\Omega_{ij}(t)$ and controlling $\Delta_j(t)$ has been studied extensively [15–18].

In nonlinear optics STIRAP considered here, the mechanism of control is the spatial modulation of the coupling coefficients κ_{12} and κ_{32}. This is analogous to the temporal shaping of $\varepsilon(t)$ in the atomic case. Furthermore, it is noted that single-photon resonance $\Delta_1 = \Delta_2 = 0$ is not required for STIRAP; two-photon resonance $\Delta_1 + \Delta_2 = 0$ is sufficient. However, for the remainder of this section we will consider the case of perfect phase-matching $\Delta k_1 = \Delta k_2 = 0$, analogous to the atomic single-photon resonance. Now we can justify the previously mentioned assumption that mixing processes not considered by our model are indeed insignificant due to a large phase-mismatch. Essentially, it is assumed that for any other process, with a phase-mismatch $\Delta k'$, we have $|\Delta k' - \Delta k_1|L \gg 1$ and $|\Delta k' - \Delta k_2|L \gg 1$. Thus it has a negligible effect when applying a method for achieving $\Delta k_1 = \Delta k_2 = 0$ to a good approximation. This assumption can be easily satisfied by considering the dispersion of the nonlinear crystal and choosing appropriate input and pumps wavelengths.

An analysis of nonlinear optics STIRAP will now be given in a manner completely analogous to the standard analysis given in the atomic case [10,11]. The three eigenvalues of the coupling matrix M are

$$\kappa_0 = 0, \qquad \kappa_\pm = \pm\sqrt{\kappa_{12}\kappa_{21} + \kappa_{23}\kappa_{32}}, \tag{3}$$

and their corresponding normalized eigenvectors are

$$|g_0\rangle = \frac{1}{\kappa_c}\begin{bmatrix}\kappa_{32}\\ 0\\ \kappa_{32}\end{bmatrix}, \qquad |g_\pm\rangle = \frac{1}{\sqrt{\kappa_c^2 + \kappa_s^2}}\begin{bmatrix}\kappa_{12}\\ \mp\kappa_s\\ \kappa_{32}\end{bmatrix}, \tag{4}$$

where we have defined $\kappa_c = \sqrt{\kappa_{12}^2 + \kappa_{32}^2}$ and $\kappa_s = \sqrt{\kappa_{12}\kappa_{21} + \kappa_{23}\kappa_{32}}$. Next, let us define the angle θ:

$$\theta \equiv \tan^{-1}\left(\frac{\kappa_{12}}{\kappa_{32}}\right). \tag{5}$$

$|g_0\rangle$ can now be written as

$$|g_0\rangle = \begin{bmatrix}\cos\theta\\ 0\\ -\sin\theta\end{bmatrix}. \tag{6}$$

This eigenvector has an important property: It has no contribution from the intermediate state, i.e., $\langle g_0|A_2\rangle = 0$. It is this property that will enable energy to be transferred from A_1 to A_3 without going through A_2, as will now be explained.

We assume that initially all of the optical power is in A_1, and additionally $|\kappa_{12}|, |\kappa_{21}| \ll |\kappa_{23}|, |\kappa_{32}|$, so $\theta \approx 0$. In this situation, out of the three eigenstates, only $|g_0\rangle$ has a nonzero term; thus the system can be said to be in this eigenstate. During the interaction, the coupling coefficients change adiabatically, such that at its end $|\kappa_{12}|, |\kappa_{21}| \ll |\kappa_{23}|, |\kappa_{32}|$, so $\theta \approx \pi/2$. According to the adiabatic theorem, if the system is at an eigenstate and is subject only to adiabatic changes, it will remain at the same eigenstate, in this case $|g_0\rangle$. However, when $\theta \approx \pi/2$, the physical meaning of $|g_0\rangle$ is that all of the optical power is in A_3. We therefore conclude that the system will remain in the $|g_0\rangle$ eigenstate throughout the interaction, going from the initial state $[1,0,0]^T$ (all power in A_1) to the final state $[0,0,-1]^T$ (all power in A_3). Since $|g_0\rangle$ contains no component of the intermediate frequency amplitude, this means that power will be transferred from A_1 to A_3 without ever going through A_2. Note that the counterintuitive order is maintained in the nonlinear optics case: First A_2 and A_3 are coupled, and the coupling between A_1 and A_2 is introduced at a later point.

In order to satisfy the adiabatic condition, it is required that the coupling between the desired eigenstate, $|g_0\rangle$, and the other eigenstates, $|g_\pm\rangle$, is small compared to the difference between the effective wavenumbers of these states [11]:

$$\left|\left\langle\frac{dg_0}{dz}\middle|g_\pm\right\rangle\right| \ll |\kappa_0 - \kappa_\pm|. \tag{7}$$

This condition can be written in terms of θ as

$$\left|\frac{d\theta}{dz}\right| \ll \frac{\kappa_s}{\kappa_c\sqrt{\kappa_c^2 + \kappa_s^2}}, \tag{8}$$

where θ is the adiabatically varying parameter, going from 0 to $\pi/2$.

While not necessarily optimal, a Gaussian modulation of the nonlinear coupling in space (along the interaction) will be used here, since it is convenient for analysis and illustrates the main features of STIRAP. For this purpose we replace the coupling coefficients in the matrix M of Eq. (2) with

$$\tilde{\kappa}_{12}(z) = \kappa_{12}e^{-(z-L/2-s)^2/w^2}$$
$$\tilde{\kappa}_{32}(z) = \kappa_{32}e^{-(z-L/2+s)^2/w^2}, \tag{9}$$

where s and w are parameters that determine the locations of coupling maxima and the rate of the coupling variation, respectively. See Fig. 2 for an illustration of these modulation functions. Note that the s parameter determines the coupling order: For $s < 0$ the intuitive order is obtained, while for $s > 0$ the modulation is in the counterintuitive order regime. Additionally, as before, $\tilde{\kappa}_{ij} = (\omega_i^2 k_j/\omega_j^2 k_i)\tilde{\kappa}_{ji}^*$.

3. NUMERICAL SIMULATION UNDER IDEAL CONDITIONS

A. Interaction in the Absence of Absorption

In this section the main features of optical STIRAP will be demonstrated by numerical simulation, which solves Eq. (1). For this purpose, it will be assumed that both processes are simultaneously phase-matched, and that the desired modulation of the coupling coefficient $\tilde{\kappa}_{ij}$ has been achieved. In this respect, the conditions are considered ideal. Section 4 will discuss a technique to imitate this situation using currently available technology.

In the simulation, the two processes were SFG and DFG: $(\lambda_1 = 3000\text{ nm}) + (\lambda_{p_1} = 800\text{ nm}) \rightarrow (\lambda_2 = 631.6\text{ nm})$ and $(\lambda_2 = 631\text{ nm}) - (\lambda_{p_2} = 1000\text{ nm}) \rightarrow (\lambda_3 = 1714\text{ nm})$. The nonlinear medium was a 35 mm long $KTiOPO_4$ (KTP) crystal with $\chi^{(2)}(\omega_1, \omega_{p_1}; \omega_2) \approx \chi^{(2)}(\omega_2, \omega_{p_2}; \omega_3) = 16.65\text{ pm/V}$ [19].

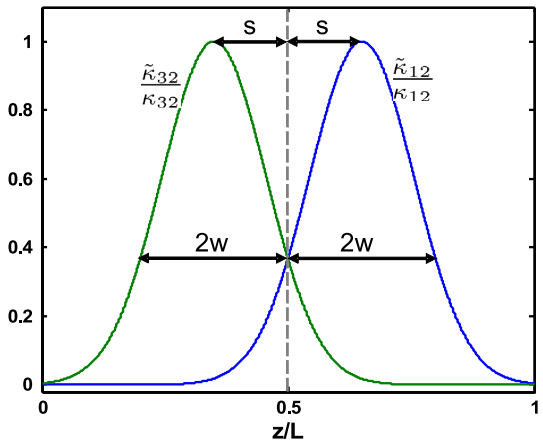

Fig. 2. (Color online) Normalized coupling coefficients of the two nonlinear processes with Gaussian modulation. Note that the $\omega_2 \leftrightarrow \omega_3$ coupling is (counterintuitively) maximized before that of $\omega_1 \leftrightarrow \omega_2$.

The coupling coefficients refractive indexes were calculated using the Sellmeier equation of Fradkin *et al.* [20] and Emanueli *et al.* [21] at a temperature of 100°C. All other three-wave mixing processes involving these wavelengths, including second harmonic generation, were verified to satisfy the assumption that they are far from phase-matching. We emphasize that, due to the dispersive nature of known second-order nonlinear crystals, this objective is practically trivial to achieve. For example, for the SFG process ($\lambda_1 = 3000$ nm) + ($\lambda_{p_2} = 1000$ nm) → ($\lambda_4 = 750$ nm) we have $|\Delta k' - \Delta k_1|L = 10^4 \gg 1$ and $|\Delta k' - \Delta k_2|L = 1.2 \times 10^4 \gg 1$. The modulation parameters were chosen to be $s = 5$ mm and $w = 8$ mm. Note that for every $s > 0$ the interaction was performed using the counterintuitive order. The input intensity was 100 MW/cm^2 and each of the two pumps had an intensity of 2 GW/cm^2. Figure 3 shows the resulting intensities of the interacting waves along the nonlinear crystal, with the intermediate wave intensity on a smaller scale in the inset. The input power is seen to be fully converted to the output wave, with some additional power from the first pump: If every photon at λ_1 is converted to a photon at λ_3, the intensity ratio is $I_3/I_1 = \omega_3/\omega_1 = \lambda_1/\lambda_3$. For the parameters used here, full conversion means $I_3 = 175$ MW/cm^2. Furthermore, the intermediate power is at most 0.8% of the input power. These are exactly the characteristics of STIRAP.

Interestingly, using the method of adiabatic elimination [9] for the same set of parameters and under the same ideal conditions, the output intensity would reach only 73.5 MW/cm^2. Clearly, the STIRAP analog method introduced here is more efficient, while maintaining the property of negligible intermediate frequency power.

For comparison, we repeated the same simulation with $s = -5$ mm, i.e., with intuitive order. The results are depicted in Fig. 4, showing strong oscillations of all three waves intensities. Specifically, significant energy is present in the intermediate frequency, in contrast to the counter-intuitive result of Fig. 3.

Furthermore, we explored the conversion process dynamics as a function of the shift parameter s. In order to do this, the width parameter was kept constant at $w = 8$ mm while the shift parameter was varied from −20 mm to +20 mm. Efficient conversion from λ_1 to λ_3 together with negligible (<1%) power at λ_2 was obtained for 3.3 mm $< s <$ 6.6 mm. In this shift interval, which is in the counterintuitive regime, the overlap

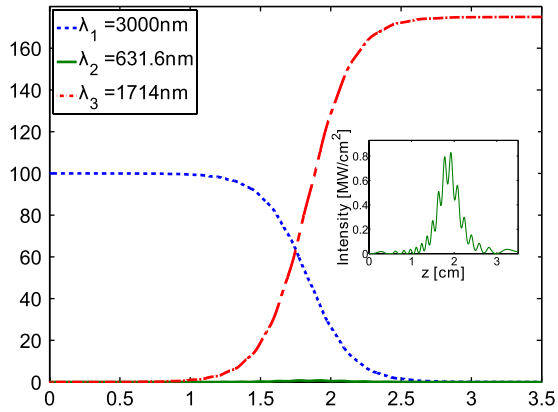

Fig. 3. (Color online) Numerical simulation of the intensities of the interacting waves along the nonlinear medium, with no intermediate wave absorption, under ideal conditions and counterintuitive order modulation ($s = 5$ mm). The inset shows the intermediate wave intensity on a smaller scale.

between the modulation Gaussians of Eq. (9) is significant enough to facilitate STIRAP. It was also found that for values of $s < 0$, i.e., in the intuitive regime, there is always high intermediate power somewhere along the crystal.

B. Interaction in the Presence of Intermediate Frequency Absorption

One of the key advantages of having a dark intermediate state is that the crystal absorption in the intermediate wavelength does not change the conversion efficiency [9]. Here we consider the same interaction as the previous one, except that the intermediate frequency is in the ultraviolet absorption band of the KTP crystal. The two processes are ($\lambda_1 = 546.5$ nm) + ($\lambda_{p_1} = 900$ nm) → ($\lambda_2 = 340$ nm) and ($\lambda_2 = 340$ nm) − ($\lambda_{p_2} = 2266$ nm) → ($\lambda_3 = 400$ nm). As in the previous case, all other three-wave mixing processes involving these wavelengths were verified to be far from phase-matching. The linear absorption coefficient at the intermediate wavelength is $\alpha_2 = 229.9$ cm^{-1} [22]. Absorption is known to be accompanied by enhancement of the nonlinear susceptibility, and this is the case here as well. However, this enhancement is not very high, since only one wavelength (λ_2) in each interaction is near an electronic transition resonance of the KTP crystal. We

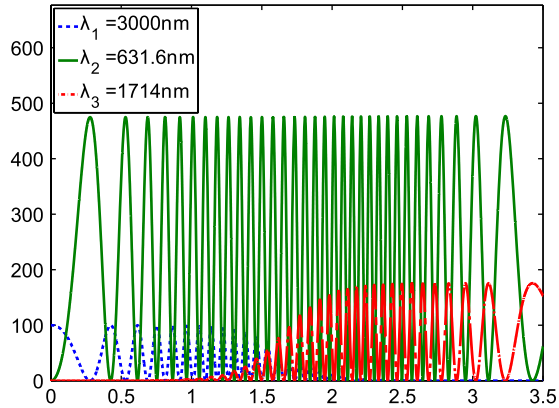

Fig. 4. (Color online) Numerical simulation of the intensities of the interacting waves along the nonlinear medium, with no intermediate wave absorption, under ideal conditions and intuitive order modulation ($s = -5$ mm).

can calculate this enhancement using the density matrix quantum mechanical model of the linear and nonlinear susceptibilities [1], which yields

$$\chi^{(1)}(\omega) \propto (\omega' - \omega - i\gamma')^{-1} \tag{10}$$

$$\chi^{(2)}(\omega_j, \omega_k; \omega_j + \omega_k) \propto (\omega' - \omega_j - \omega_k - i\gamma')^{-1} \times [(\omega'' - \omega_j - i\gamma'')^{-1} + (\omega''' - \omega_k - i\gamma''')^{-1}]. \tag{11}$$

Here the primed ω and γ terms are resonant transition frequencies and full widths at half maximum, respectively, and ω_j and ω_k are the two low frequencies out of the three in the TWM process. In the case under study, each of the two low frequencies in each of the two processes, namely ω_1, ω_{p_1}, ω_{p_2}, and ω_3, are far from any resonance. The last two terms of Eq. (11) therefore do not contribute to the resonant enhancement of $\chi^{(2)}$. The enhancement stems only from the first term, since it refers to the high frequency which is the intermediate frequency ω_2 in each of the two processes considered here. From Eqs. (10) and (11) it is therefore clear that in this case the second order susceptibility scales like the first order susceptibility. The enhancement factor for the wavelengths involved here can be calculated using the relation between the linear susceptibility and the refractive index, by making use of the Sellmeier equation of KTP:

$$\frac{\chi^{(2)}(\lambda_1 + \lambda_{p_1} \to \lambda_2)}{\chi^{(2)}(1064\text{ nm} + 1064\text{ nm} \to 532\text{ nm})} = \frac{\chi^{(2)}(\lambda_2 - \lambda_{p_2} \to \lambda_3)}{\chi^{(2)}(1064\text{ nm} + 1064\text{ nm} \to 532\text{ nm})} = \frac{\chi^{(1)}(\lambda_2)}{\chi^{(1)}(1064\text{ nm})} = \frac{n^2(\lambda_2) - 1}{n^2(1064\text{ nm}) - 1} = 1.4, \tag{12}$$

where we have used the 1064 nm second harmonic generation value of $\chi^{(2)}$ as a reference. This enhancement is equivalent to increasing the intensity of each of the two pumps by a factor of $1.4^2 \approx 2$.

In addition to linear absorption, when photon energies higher than half the band-gap energy are involved, two-photon absorption (TPA) should also be taken into account. According to DeSalvo *et al.* effective bandgap model for KTP [23], TPA involving two photons with energies $\hbar\omega_a$ and $\hbar\omega_b$ is negligible for $\hbar(\omega_a + \omega_b) < 4.6$ eV, which corresponds to a wavelength of 270 nm. Consequently, in our case, TPA is significant only for λ_2 and λ_3, which have TPA coefficients of $\beta_2 = 2.53$ cm/GW and $\beta_3 = 2.62$ cm/GW, respectively. In order to avoid TPA effects, we use an input intensity of 10 MW/cm^2 for this case.

Using these parameters together with the same pump intensities and Gaussian modulation of the coupling coefficients as before, Eq. (1) was solved once again. Linear absorption and TPA were integrated into Eq. (1) by the simple substitution $M_{ij} \to M_{ij} - \alpha_i A_i - \beta_i I_i$, where $I_i = 2n_i(\omega_i)\epsilon_0 c|A_i|^2$ is the intensity of the wave with frequency ω_i. The resulting intensities along the crystal are displayed in Fig. 5, which shows that the conversion from λ_1 to λ_3 is still efficient, peaking at 95.8% (here full conversion means $I_3 = 13.66$ MW/cm^2 due to contribution from the first pump). This result reveals the true merit of avoiding significant power at the intermediate

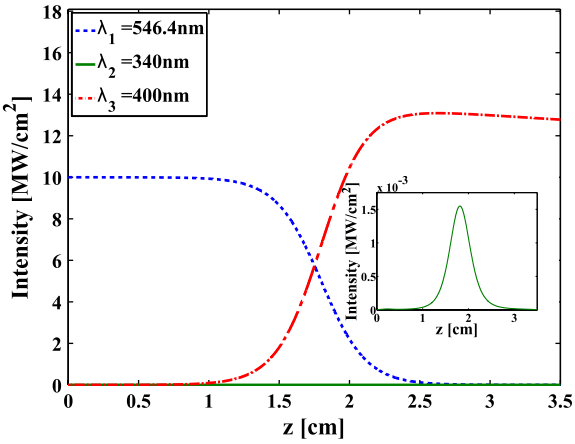

Fig. 5. (Color online) Numerical simulation of the intensities of the interacting waves along the nonlinear medium, with high intermediate wave absorption and under ideal conditions. The inset shows the intermediate wave intensity on a smaller scale.

frequency, as it allows the conversion to remain efficient in spite of great absorption at λ_2. The intermediate frequency absorption has two observable effects: (i) the maximum conversion efficiency was below 100% since some power was still lost (ii) the intermediate wave intensity, displayed in the inset of Fig. 5, reaches at most 0.015% of the input intensity (compare with 0.8% for the case with no absorption; see Fig. 3). The slight decay of the output intensity toward the end of the crystal is attributed to TPA.

As a final note in this section, we emphasize once more that nonlinear processes involving resonant excitation of atoms or ions [12] are not relevant here. The radiative contribution of atoms excited by linear or nonlinear absorption is negligible compared to the nonlinear processes.

4. NUMERICAL SIMULATION USING PHASE-REVERSAL QUASIPHASE-MATCHING

In the preceding section it was assumed that both processes were phase matched and that the coupling coefficients were modulated as desired, without accounting for any mechanism to achieve these purposes. Now these assumptions will not be made. Instead, a technique called phase-reversal quasi-phase matching (PRQPM) [7] will be employed to provide phase-matching as well as to modulate the coupling coefficients. In PRQPM, binary functions are multiplied to produce a desired modulation, which has multiple Fourier components. This modulation can therefore provide QPM for multiple processes, i.e., processes with different phase-mismatches. For example, we can construct a product of two binary functions as follows:

$$g(z) = \text{sign}\left[-\cos(\pi D_1) + \cos\left(\frac{2\pi}{\Lambda_1}z\right)\right] \times \text{sign}\left[-\cos(\pi D_2) + \cos\left(\frac{2\pi}{\Lambda_2}z\right)\right]. \tag{13}$$

For each periodic term in the product, D_j is the duty cycle and Λ_j is the period. As always in QPM, we keep only the first order Fourier terms that contribute the desired phase-mismatches. If we choose $\Lambda_1 = \Delta k_1$ and $\Lambda_2 = \Delta k_2$, using simple Fourier analysis yields

$$g_{\mathrm{QPM}}(z) \approx \frac{2}{\pi}(2D_2 - 1)\sin(\pi D_1)\exp(\pm i\Delta k_1) + \frac{2}{\pi}(2D_1 - 1)\sin(\pi D_2)\exp(\pm i\Delta k_2). \quad (14)$$

This is the modulation of $\chi^{(2)}$, i.e., $\chi^{(2)} \to g_{\mathrm{QPM}}\chi^{(2)}$, and $\kappa_{ij} \propto \chi^{(2)}$. The first (second) term in the sum therefore phase-matches the first (second) process. This can be understood by looking at the matrix of Eq. (2), which now becomes

$$M' \approx -\frac{2}{\pi}\begin{bmatrix} 0 & (2D_2 - 1)\sin(\pi D_1)\kappa_{12} & 0 \\ (2D_2 - 1)\sin(\pi D_1)\kappa_{21} & 0 & (2D_1 - 1)\sin(\pi D_2)\kappa_{23} \\ 0 & (2D_1 - 1)\sin(\pi D_2)\kappa_{32} & 0 \end{bmatrix}, \quad (15)$$

where we have only kept phase-matched terms. Evidently, this choice of the modulation periods provides QPM for the desired processes, while D_1 and D_2 determine the magnitude of the effective coupling coefficient for each process. Varying the two duty cycles along the crystal achieves the required modulation.

The two cases regarded in Section 3, with ideal phase-matching and coefficient modulation, are considered again in this section. In addition to using PRQPM for phase-matching and coefficient modulation, the calculation made here also takes into consideration technological restrictions on nonlinear modulation, and pumps depletion/amplification. We shall now assume that QPM is achieved by the widespread technique of electric field poling of a ferroelectric crystal.

Using QPM, especially when considering the technological limitations of this technique, makes it more difficult to satisfy the adiabaticity condition of Eq. (8), which essentially requires the changes in the coefficients to be very gradual. For this purpose, we first note that the spatial area where $\tilde{\kappa}_{32}$ is rising while $\tilde{\kappa}_{12} \approx 0$ is going to waste, since $\theta = 0$ all along it (see Fig. 2). In order to achieve adiabatic interaction, it is sufficient that at the start $\tilde{\kappa}_{12} \ll \tilde{\kappa}_{32}$. We can therefore start the interaction with $\tilde{\kappa}_{32}(0) = \max[\tilde{\kappa}_{32}(z)]$, i.e., by choosing $s = L/2$, and use the additional space, which was previously wasted, to make the coefficients gradients smaller, by increasing the modulation width w. For this reason, in the simulations conducted using PRQPM, the shift parameter was $s = L/2 = 17.5$ mm and the width parameter was $w = 25$ mm. In order to obtain the required binary modulation pattern, we numerically found the values of D_1 and D_2 that minimize the expression $(\tilde{\kappa}_{12} - |M'_{12}|)^2 + (\tilde{\kappa}_{32} - |M'_{32}|)^2$ at each point along the interaction. The resulting normalized coefficients are displayed in Fig. 6, along with an example of a corresponding PRQPM poling pattern at various locations.

Furthermore, we note that Zukauskas *et al.* succeeded in fabricating domains as small as 345 nm in KTP [24]. In the simulation conducted here, domains formed by Eq. (13), which were less than 350 nm long, were concatenated with neighboring domains until they reached this minimum length. In this manner modulation patterns that are attainable with current technology have been constructed.

Simulation results for the first set of wavelengths, all of which are in the crystal's transparency spectral region, are displayed in Fig. 7. Comparing with the ideal case results shown in Fig. 3, we see that the main features of the interaction have been preserved: High conversion from λ_1 to λ_3 is obtained, while the intermediate wavelength intensity remains relatively low. Still, there are two clear differences from the ideal case: The intermediate intensity reaches a higher value (9.15% of the input) and the intensities of all three waves fluctuate along the crystal. Both of these differences come from the use of PRQPM and the domain size limit: The oscillations are a well-established property of QPM, coming from the non-phase-matched part of the interaction, i.e., higher Fourier orders of the modulation. The desired adiabatic variation is obtained on an average scale, which includes many domains. As a result, on a shorter scale, energy does get transferred to the intermediate wave. The modulation periods being $\Lambda_1 = 18.2$ μm and $\Lambda_1 = 15.5$ μm, the domain size limit makes it more difficult to satisfy the adiabatic condition, resulting in more energy transfer to λ_2.

Simulation results for the second set of wavelengths, which include a highly absorbed intermediate wave, are depicted in

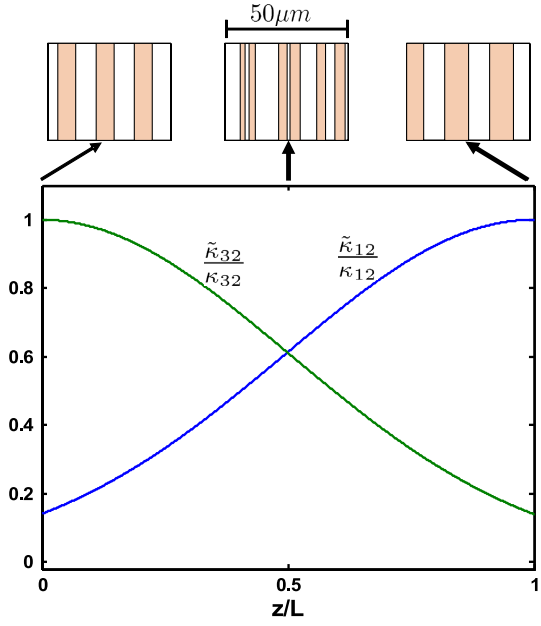

Fig. 6. (Color online) Normalized coupling coefficients of the two nonlinear processes with the modulation used in Section 4. The top panels show the PRQPM poling, which was used in the simulation of Fig. 7, at the beginning, center and end of the nonlinear crystal. The colored and white stripes represent domains with positive and negative nonlinearity.

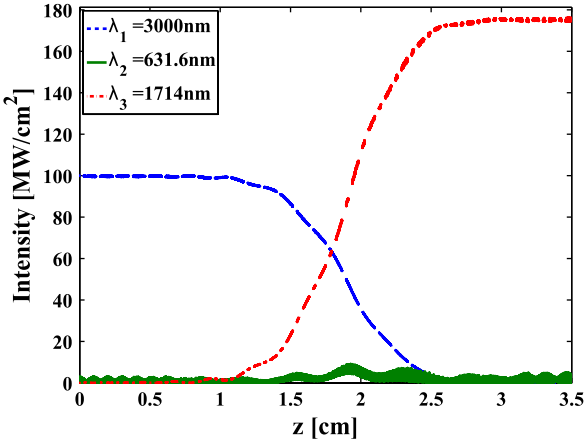

Fig. 7. (Color online) Numerical simulation of the intensities of the interacting waves along the nonlinear medium, with no intermediate wave absorption and where the crystal is modulated using phase-reversal quasi-phase-matching.

Fig. 8. While significant conversion from λ_1 to λ_3 took place in this case, it has some features which clearly distinguish it from the ideal case, in addition to the usual QPM oscillations noted above. First, the intermediate intensity reaches a value as high as 5.8% of the input intensity, where significant intermediate power is only present in two confined spatial areas. The reason for this phenomenon is that in these areas the domain size limitation causes loss of adiabaticity, resulting in energy transfer from λ_1 and λ_3 to λ_2, which is quickly absorbed by the crystal. Note that the modulation periods are $\Lambda_1 = 1.69$ μm and $\Lambda_2 = 2.73$ μm, so small domains are abundant. Because of the loss of adiabaticity, the remainder of the interaction is also characterized by conversion from λ_1 and λ_3 to λ_2, albeit at a slower rate since little energy is present at the intermediate frequency at any point, due to the strong absorption. The overall conversion efficiency is reduced by a factor of 2.3 compared to the ideal case, but is still considerable in face of the strong absorption of λ_2.

Optical STIRAP via PRQPM, in the presence of intermediate frequency absorption, is ultimately limited by the ratio between the absorption length $l_{\text{abs}} = 1/\alpha_2$ and the natural coherence lengths $l_c^{(j)} = \pi/\Delta k_j$, $j = 1, 2$ [1], where here Δk_j is the natural phase-mismatch (i.e., as resulting from dispersion, without any QPM compensation). In order for any QPM scheme to have a significant effect, it is required that $l_{\text{abs}} > l_c$; otherwise an interacting wave will be absorbed before being affected by the modulation (for the case considered here, we have $l_{\text{abs}}/l_c^{(1)} = 51.5$ and $l_{\text{abs}}/l_c^{(2)} = 31.9$). Nevertheless, optical STIRAP via PRQPM still greatly reduces the conversion efficiency's sensitivity to intermediate frequency absorption, since considerably less energy is ever present in the intermediate wave. Furthermore, no critical control of the modulation is required, as is the case for nonadiabatic QPM methods in the presence of absorption, which significantly limits the interaction length. Nevertheless, when venturing into the UV absorption band, care must be taken to avoid TPA of any but the intermediate wave. The pumps wavelengths and input intensities need to be chosen such that TPA is not significant.

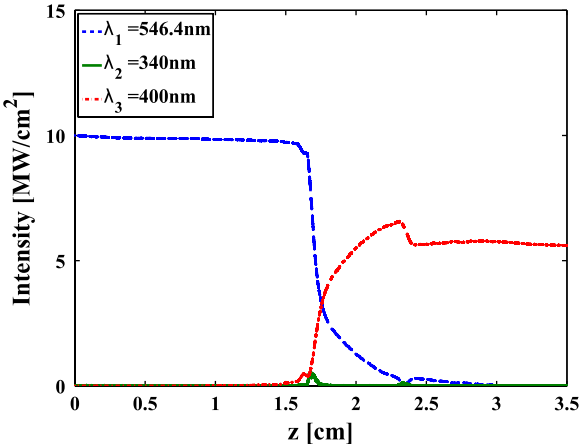

Fig. 8. (Color online) Numerical simulation of the intensities of the interacting waves along the nonlinear medium, with high intermediate wave absorption and where the crystal is modulated using phase-reversal quasi-phase-matching.

An additional limitation of this modulation scheme is that in order to achieve independent control of each of the two processes via the duty cycles D_1 and D_2, their phase-mismatches need to be sufficiently different from one another. Otherwise, each of the two terms in Eq. (14) will have the same effect on both processes, and independent control would be lost.

Finally, we note that the acceptance bandwidth of this scheme would be the same as any PRQPM device [7]. It is possible that methods for extending QPM bandwidth [5,13] could be used here as well, however this issue is beyond the scope of this paper.

5. FUTURE PROSPECTS AND APPLICATIONS

In the previous section, limitations of PRQPM in face of current fabrication capabilities were discussed. Specifically, it was demonstrated that the minimum domain size limits this method's capability of satisfying the adiabaticity condition when the dispersion is stronger, i.e., when the interacting wavelengths are relatively short (in the near UV). We consider it reasonable to assume that the current trend of ever decreasing available domain size will continue [24], making PRQPM feasible to processes involving short wavelengths, going into the UV. Note also that the domain size limitation can be somewhat circumvented, by relinquishing single photon resonance $\Delta k_1 = \Delta k_2 = 0$ and satisfying only two photon resonance $\Delta k_1 + \Delta k_2 = 0$. However, this will come at a cost of efficiency because, in general, the power transfer rate of a nonlinear process decreases with increasing phase-mismatch for fixed pump intensity [1,9].

Moreover, conversion efficiency can be further improved by employing techniques originally invented for atomic STIRAP [15–18]. In these techniques the temporal dependence of the Rabi frequencies and detunings are controlled by pulse shaping and chirping mechanisms, respectively. Both of these controls have counterparts in PRQPM optical STIRAP. As was shown here, the coupling coefficients can be controlled via the duty cycles of the PRQPM modulation function of Eq. (14), in analogy with pulse shaping of the Rabi frequencies. Additionally, the effective phase-mismatch of each process can be modulated along the interaction by variations in the periods of the modulation (Λ_1 and Λ_2 in Eq. (14)). This is the counterpart of variable atomic detunings, obtained by chirping.

An entirely different method for obtaining adiabatic interaction can involve anomalous dispersion phase-matching (ADPM) and tight beam focusing. In ADPM, absorption resonances are deliberately brought forth, either by doping bulk nonlinear crystals with metals or ions [25], or by introducing chromophores in the fabrication process of polymer waveguides [26]. These resonances influence the dispersion properties of the nonlinear medium, thus enabling birefringent phase-matching of various processes. Nonlinear optics STIRAP can be facilitated by using ADPM for phase-matching, while focusing the two pump beams at different locations along the crystal, achieving the modulation of the coupling coefficients simply by allowing diffraction to modulate pumps intensities (working with focused beams would invalidate the plane-wave approximation used in this work; however we believe that this would not prevent our method from being applied, and that it can be compensated by increasing pump power). Furthermore, the intermediate frequency can reside within the absorption band of the doped crystal without hindering the conversion efficiency.

Two applications of nonlinear optics STIRAP will now be put forth. First, a straightforward application would simply be frequency conversion across large frequency ranges or between near frequencies. By employing two SFG or two DFG processes, efficient conversion can be performed where the input and output frequencies are greatly separated from each other (e.g., mid-IR input and blue visible output, or vice versa). If a SFG process is used together with a DFG process, where the two pumps frequencies are close to each other, upconversion or downconversion to a frequency near that of the input would be achieved. The merit of STIRAP is that these objectives can be achieved with TWM without requiring lasers that have very high (low) frequencies that bridge the gap between very far (near) frequencies, as such lasers are scarcely available at the power level required for nonlinear processes. Second, we suggest that this method can be employed in the study of nonlinear crystal electronic structure and properties, by employing a SFG process followed by a DFG process. While Raman spectroscopy enables the study of molecular structure in the infrared absorption band, experimental data on the electronic structure in the UV absorption band is scarce [19,27]. Experiments to this effect rely mostly on nonlinear absorption and refraction [23,28], and are limited by linear absorption. UV electronic resonances will have a significant influence on nonlinear optics STIRAP processes, first via phase-matching and second via enhancement of the nonlinear coefficient. For example, by using a tunable pump or by tuning the crystal temperature, phase matching conditions can be controlled, thus allowing direct measurement of dispersion inside the UV absorption band.

6. CONCLUSION

This work theoretically demonstrates a method for efficient frequency conversion through an intermediate frequency, which never receives any significant amount of power throughout the interaction. This property was predicted analytically by analogy with atomic STIRAP, and confirmed with numerical simulations. It was shown that the absence of power at the intermediate frequency renders the conversion efficiency highly insensitive to absorption of the intermediate frequency, opening the way to conversion through absorptive bands in the UV. A technologically feasible method for carrying out such a process was proposed and numerically demonstrated to be effective. We suggest applying this method in conversion between highly disparate frequencies, e.g., mid-IR to visible conversion. Another application is the study of the electronic structure and properties of nonlinear optical crystals, which is manifested in the UV absorption band, now made accessible in spite of linear absorption.

ACKNOWLEDGMENTS

The authors would like to thank Dr. Haim Suchowski and Dr. Ori Katz for fruitful discussions. This work was supported by the Israel Science Foundation.

REFERENCES

1. R. W. Boyd, *Nonlinear Optics*, 3rd ed. (Academic, 2008).
2. S. M. Saltiel, A. A. Sukhorukov, and Y. S. Kivshar, "Multistep parametric processes in nonlinear optics," Prog. Opt. **47**, 1–73 (2005).
3. A. Tehranchi, R. Morandotti, and R. Kashyap, "Efficient flattop ultra-wideband wavelength converters based on double-pass cascaded sum and difference frequency generation using engineered chirped gratings," Opt. Express **19**, 22528–22534 (2011).
4. J. A. Armstrong, N. Bloembergen, J. Ducuing, and P. S. Pershan, "Interactions between light waves in a nonlinear dielectric," Phys. Rev. **127**, 1918–1939 (1962).
5. D. S. Hum and M. M. Fejer, "Quasi-phasematching," C. R. Phys. **8**, 180–198 (2007).
6. R. Lifshitz, A. Arie, and A. Bahabad, "Photonic quasicrystals for nonlinear optical frequency conversion," Phys. Rev. Lett. **95**, 133901 (2005).
7. M. H. Chou, K. R. Parameswaran, M. M. Fejer, and I. Brener, "Multiple-channel wavelength conversion by use of engineered quasi-phase-matching structures in $LiNbO_3$ waveguides," Opt. Lett. **24**, 1157–1159 (1999).
8. S. Longhi, "Third-harmonic generation in quasi-phase-matched $\chi^{(2)}$ media with missing second harmonic," Opt. Lett. **32**, 1791–1793 (2007).
9. G. Porat, Y. Silberberg, A. Arie, and H. Suchowski, "Two photon frequency conversion," Opt. Express **20**, 3613–3619 (2012).
10. D. Tannor, *Introduction to Quantum Mechanics: A Time-Dependent Perspective* (University Science Books, 2007).
11. N. V. Vitanov, T. Halfmann, B. W. Shore, and K. Bergmann, "Laser-induced population transfer by adiabatic passage techniques," Annu. Rev. Phys. Chem. **52**, 763–809 (2001).
12. F. Auzel, "Upconversion and anti-Stokes processes with f and d ions in solids," Chem. Rev. **104**, 139–174 (2004).
13. H. Suchowski, D. Oron, A. Arie, and Y. Silberberg, "Geometrical representation of sum frequency generation and adiabatic frequency conversion," Phys. Rev. A **78**, 063821 (2008).
14. H. Suchowski, B. D. Bruner, A. Ganany-Padowicz, I. Juwiler, A. Arie, and Y. Silberberg, "Adiabatic frequency conversion of ultrafast pulses," Appl. Phys. B **105**, 697–702 (2011).
15. T. A. Laine and S. Stenholm, "Adiabatic processes in three-level systems," Phys. Rev. A **53**, 2501–2512 (1996).
16. G. S. Vasilev, A. Kuhn, and N. V. Vitanov, "Optimum pulse shapes for stimulated Raman adiabatic passage," Phys. Rev. A **80**, 013417 (2009).
17. G. Dridi, S. Gurin, V. Hakobyan, H. R. Jauslin, and H. Eleuch, "Ultrafast stimulated Raman parallel adiabatic passage by shaped pulses," Phys. Rev. A **80**, 043408 (2009).
18. Xi Chen, I. Lizuain, A. Ruschhaupt, D. Gury-Odelin, and J. G. Muga1, "Shortcut to adiabatic passage in two-and three-level atoms," Phys. Rev. Lett. **105**, 123003 (2010).
19. A. H. Reshak, I. V. Kityk, and S. Auluck, "Investigation of the linear and nonlinear optical susceptibilities of $KTiOPO_4$ single crystals: theory and experiment," J. Phys. Chem. B **114**, 16705–16712 (2010).
20. K. Fradkin, A. Arie, A. Skliar, and G. Rosenman, "Tunable mid-infrared source by difference frequency generation in bulk periodically poled $KTiOPO_4$," Appl. Phys. Lett. **74**, 914–916 (1999).

21. S. Emanueli and A. Arie, "Temperature-dependent dispersion equations for $KTiOPO_4$ and $KTiOAsO_4$," Appl. Opt. **42**, 6661–6665 (2003).
22. A. Dudelzak, P. P. Proulx, V. Denks, V. Murk, and V. Nagirnyi, "Anisotropic fundamental absorption edge of $KTiOPO_4$ crystals," J. Appl. Phys. **87**, 2110–2113 (2000).
23. R. DeSalvo, A. A. Said, D. J. Hagan, E. W. Van Stryland, and M. Sheik-Bahae, "Infrared to ultraviolet measurements of two-photon absorption and n_2 in wide bandgap solids," IEEE J. Quantum Electron. **32**, 1324–1333 (1996).
24. A. Zukauskas, G. Strömqvist, V. Pasiskevicius, F. Laurell, M. Fokine, and C. Canalias, "Fabrication of submicrometer quasi-phasematched devices in KTP and RKTP," Opt. Mater. Express **1**, 1319–1325 (2011).
25. M. T. Anderson, M. L. F. Phillips, M. B. Sinclair, and G. D. Stucky, "Synthesis of transition-metal-doped $KTiOPO_4$ and lanthanide-doped $RbTiOAsO_4$ isomorphs that absorb visible light," Chem. Mater. **8**, 248–256 (1996).
26. R. Dietrich, K. Meerholz, C. Brauchle, J. Wichern, and P. Boldt, "Phase-matched second-harmonic generation due to anomalous dispersion: tailoring of the refractive indices in three-component systems," Chem. Phys. Lett. **280**, 119–126 (1997).
27. S. Cabuk, "The nonlinear optical susceptibility and electro-optic tensor of ferroelectrics: first-principle study," Cent. Eur. J. Phys. **10**, 239–252 (2012).
28. H. Li, F. Zhou, X. Zhang, and W. Ji, "Bound electronic Kerr effect and self-focusing induced damage in second-harmonic-generation crystals," Opt. Commun. **144**, 75–81 (1997).